3D Simulation of a Transonic Wing Flutter using an Efficient High Resolution Upwind Scheme

Xiangying Chen* and Ge-Cheng Zha†
Dept. of Mechanical and Aerospace Engineering
University of Miami
Coral Gables, Florida 33124

Ming-Ta Yang‡
Discipline Engineering - Structures
Pratt & Whitney
400 Main Street, M/S 163-07
East Hartford, CT 06108

Abstract

The flutter boundary of the 3D AGARD 445.6 Wing is calculated by using an efficient upwind scheme, Zha CUSP2, in moving grid system. The 3D Reynolds average Navier-Stokes equations are solved. Closure of the Reynolds stresses is provided by the Baldwin-Lomax turbulence model. The modal approach solver is used to calculate the structural response under aerodynamic forces with second-order accuracy. The CFD and structural solvers are fully coupled implicitly via successive iterations within each physical time step. The numerical results show that this method is capable of capturing the aeroelastic properties of the flexible wing efficiently. The computed flutter boundary of AGARD Wing 445.6 for free stream Mach numbers ranging from 0.499 to 1.141 agrees well with the experiment.

1   Introduction

Particular attention needs to be paid for simulation of 3-D flow-induced structural vibration in a transonic flow since it is a very CPU time consuming task and the dynamic response of the system is sensitive to the numerical dissipation introduced by the numerical scheme. Consequently, it's required that the numerical scheme is able to model the flow field with high efficiency and low numerical diffusion.

Among many researchers in the field of aeroelastic analysis of 3-D flexible structures, Lee-Rausch and Batina[1] used a three-factor, implicit, upwind-biased Euler/Navier-Stokes code coupled with a modal structure solver. Morton, Melville and Gordnier et al. developed an implicit fully coupled fluid-structure interaction model, which used a Beam-Warming implicit, approximate factored scheme for the flow solver coupled with modal structural solver [2][3][4][5]. Liu et al. developed a

---

* Research Associate
† Associate Professor
‡ Principal Engineer

fully coupled method using Jameson's explicit scheme with multigrid method and a modal structural model[6]. Doi and Alonso[7] coupled a explicit Runge-Kutta multigrid flow solver with a FEM structure solver to predict the aeroelastic responses of NASA Rotor 67 blade.

Recently Chen et al.[8] have developed a fully coupled methodology for calculating the flow-induced flexible body vibrations. In their method, the Roe scheme is extended to the moving grid system. The unsteady solutions march in time by using a dual-time stepping implicit unfactored Gauss-Seidel iteration. The unsteady Navier-Stokes equations and the modal structural equations are fully coupled implicitly via successive iteration within each physical time step. Comparing the methods mentioned previously, the work done by Chen et al. [8] has several following advantages given below:

(1) The unfactored Gauss-Seidel iteration is unconditionally stable and can avoid factorization error introduced by those factorized methods, such as the methods used in [1][2][3][4][5]. This feature allows very large time step to achieve fast convergence rate.

(2) Unlike the central differencing schemes used in [2] [2][3][4][5][6], the Roe scheme has inherent dissipation, and does not need additional artificial dissipation terms which need to be calibrated case by case.

(3) Modal approach structure model offers a significant CPU time savings over the FEM full structure model used in [7]. Compared with the full model results using FEM solver ANSYS, it is shown that the modal approach is very accurate for moderate deflection and torsion such as those encountered in AGARD Wing 445.6 flutter[8].

The drawback in [8] is that the Roe scheme Riemann solver consumes a lot of CPU time due to its matrix operation. To remedy this problem, a newly developed E-CUSP upwind scheme suggested by Zha [9] is employed in this paper to make the aeroelastic calculation more efficient. Same as the Roe scheme, the Zha E-CUSP2 scheme has very low diffusion and is able to capture crisp shock profiles and accurate boundary layer profiles[9]. Furthermore, this scheme is more CPU time efficient than Roe scheme since it does not require any matrix operation. The flux computational work amount of Zha E-CUSP2 scheme is only 1/4 of that of the Roe scheme [10].

In this paper, the complete flutter boundary (free stream Mach number ranging from 0.499 to 1.141) for AGARD Wing 445.6 is calculated. The computed results are presented and compared with the corresponding experimental data given in ref.[11].

2 CFD Model

2.1 Flow Governing Equations

The governing equations for the flow field computation are the Reynolds-Averaged Navier-Stokes equations (RANS) with Favre mass average which can be transformed to the generalized coordinates and expressed as:

$$\frac{\partial \mathbf{Q}'}{\partial t} + \frac{\partial \mathbf{E}'}{\partial \xi} + \frac{\partial \mathbf{F}'}{\partial \eta} + \frac{\partial \mathbf{G}'}{\partial \zeta} = \frac{1}{Re} \left(\frac{\partial \mathbf{E}'_{\mathbf{v}}}{\partial \xi} + \frac{\partial \mathbf{F}'_{\mathbf{v}}}{\partial \eta} + \frac{\partial \mathbf{G}'_{\mathbf{v}}}{\partial \zeta} \right) \tag{1}$$

where Re is the Reynolds number and

$$\mathbf{Q}' = \frac{\mathbf{Q}}{J} \tag{2}$$

$$\mathbf{E}' = \frac{1}{J}(\xi_t\mathbf{Q} + \xi_x\mathbf{E} + \xi_y\mathbf{F} + \xi_z\mathbf{G}) = \frac{1}{J}(\xi_t\mathbf{Q} + \mathbf{E}'') \tag{3}$$

$$\mathbf{F}' = \frac{1}{J}(\eta_t\mathbf{Q} + \eta_x\mathbf{E} + \eta_y\mathbf{F} + \eta_z\mathbf{G}) = \frac{1}{J}(\eta_t\mathbf{Q} + \mathbf{F}'') \tag{4}$$

$$\mathbf{G}' = \frac{1}{J}(\zeta_t\mathbf{Q} + \zeta_x\mathbf{E} + \zeta_y\mathbf{F} + \zeta_z\mathbf{G}) = \frac{1}{J}(\zeta_t\mathbf{Q} + \mathbf{G}'') \tag{5}$$

$$\mathbf{E}'_{\mathbf{v}} = \frac{1}{J}(\xi_x\mathbf{E}_{\mathbf{v}} + \xi_y\mathbf{F}_{\mathbf{v}} + \xi_z\mathbf{G}_{\mathbf{v}}) \tag{6}$$

$$\mathbf{F}'_{\mathbf{v}} = \frac{1}{J}(\eta_x\mathbf{E}_{\mathbf{v}} + \eta_y\mathbf{F}_{\mathbf{v}} + \eta_z\mathbf{G}_{\mathbf{v}}) \tag{7}$$

$$\mathbf{G}'_{\mathbf{v}} = \frac{1}{J}(\zeta_x\mathbf{E}_{\mathbf{v}} + \zeta_y\mathbf{F}_{\mathbf{v}} + \zeta_z\mathbf{G}_{\mathbf{v}}) \tag{8}$$

where the variable vector $\mathbf{Q}$, and inviscid flux vectors $\mathbf{E}$, $\mathbf{F}$, and $\mathbf{G}$ are

$$\mathbf{Q} = \begin{pmatrix} \bar{\rho} \\ \bar{\rho}\tilde{u} \\ \bar{\rho}\tilde{v} \\ \bar{\rho}\tilde{w} \\ \bar{\rho}\tilde{e} \end{pmatrix}, \quad \mathbf{E} = \begin{pmatrix} \bar{\rho}\tilde{u} \\ \bar{\rho}\tilde{u}\tilde{u} + \tilde{p} \\ \bar{\rho}\tilde{u}\tilde{v} \\ \bar{\rho}\tilde{u}\tilde{w} \\ (\bar{\rho}\tilde{e} + \tilde{p})\tilde{u} \end{pmatrix}, \quad \mathbf{F} = \begin{pmatrix} \bar{\rho}\tilde{v} \\ \bar{\rho}\tilde{u}\tilde{v} \\ \bar{\rho}\tilde{v}\tilde{v} + \tilde{p} \\ \bar{\rho}\tilde{w}\tilde{v} \\ (\bar{\rho}\tilde{e} + \tilde{p})\tilde{v} \end{pmatrix}, \quad \mathbf{G} = \begin{pmatrix} \bar{\rho}w \\ \bar{\rho}\tilde{u}\tilde{w} \\ \bar{\rho}\tilde{v}\tilde{w} \\ \bar{\rho}\tilde{w}\tilde{w} + \tilde{p} \\ (\bar{\rho}\tilde{e} + \tilde{p})\tilde{w} \end{pmatrix},$$

The $\mathbf{E}''$, $\mathbf{F}''$, and $\mathbf{G}''$ are the inviscid fluxes at the stationary grid system and are:

$$\mathbf{E}'' = \xi_x\mathbf{E} + \xi_y\mathbf{F} + \xi_z\mathbf{G},$$

$$\mathbf{F}'' = \eta_x\mathbf{E} + \eta_y\mathbf{F} + \eta_z\mathbf{G},$$

$$\mathbf{G}'' = \zeta_x\mathbf{E} + \zeta_y\mathbf{F} + \zeta_z\mathbf{G},$$

and the viscous flux vectors are given by

$$\mathbf{E}_{\mathbf{v}} = \begin{pmatrix} 0 \\ \bar{\tau}_{xx} - \overline{\rho u''u''} \\ \bar{\tau}_{xy} - \overline{\rho u''v''} \\ \bar{\tau}_{xz} - \overline{\rho u''w''} \\ Q_x \end{pmatrix}, \quad \mathbf{F}_{\mathbf{v}} = \begin{pmatrix} 0 \\ \bar{\tau}_{yx} - \overline{\rho v''u''} \\ \bar{\tau}_{yy} - \overline{\rho v''v''} \\ \bar{\tau}_{yz} - \overline{\rho v''w''} \\ Q_y \end{pmatrix}, \quad \mathbf{G}_{\mathbf{v}} = \begin{pmatrix} 0 \\ \bar{\tau}_{zx} - \overline{\rho w''u''} \\ \bar{\tau}_{zy} - \overline{\rho w''v''} \\ \bar{\tau}_{zz} - \overline{\rho w''w''} \\ Q_z \end{pmatrix}$$

In above equations, ρ is the density, u, v, and w are the Cartesian velocity components in x, y and z directions, p is the static pressure, and e is the total energy per unit mass. The overbar denotes the Reynolds-averaged quantity, tilde and double-prime denote the Favre mean and Favre fluctuating part of the turbulent motion respectively. All the flow variable in above equations are non-dimensionlized by using the freestream quantities and a reference length L.

Let subscript 1, 2 and 3 represent the coordinates, x, y, and z, and use Einstein summation convention, the shear-stress and Q_x, Q_y, Q_z terms in non-dimensional forms can be expressed in tensor form as

$$\bar{\tau}_{ij} = -\frac{2}{3}\tilde{\mu}\frac{\partial \tilde{u}_k}{\partial x_k}\delta_{ij} + \tilde{\mu}(\frac{\partial \tilde{u}_i}{\partial x_j} + \frac{\partial \tilde{u}_j}{\partial x_i}) \tag{9}$$

$$Q_i = \tilde{u}_j(\bar{\tau}_{ij} - \overline{\rho u'' u''}) - (\bar{q}_i + C_p\overline{\rho T'' u_i''}) \tag{10}$$

where the mean molecular heat flux is

$$\bar{q}_i = -\frac{\tilde{\mu}}{(\gamma - 1)Pr}\frac{\partial a^2}{\partial x_i} \tag{11}$$

The molecular viscosity $\tilde{\mu} = \tilde{\mu}(\tilde{T})$ is determined by Sutherland law, and $a = \sqrt{\gamma R T_\infty}$ is the speed of sound. The equation of state closes the system,

$$\bar{\rho}\tilde{e} = \frac{\tilde{p}}{(\gamma - 1)} + \frac{1}{2}\bar{\rho}(\tilde{u}^2 + \tilde{v}^2 + \tilde{w}^2) + k \tag{12}$$

where γ is the ratio of specific heats, k is the Favre mass-averaged turbulence kinetic energy. The turbulent shear stresses and heat flux appeared in above equations are calculated by Baldwin-Lomax model[12]. The viscosity is composed of $\mu + \mu_t$, where μ is the molecular viscosity and μ_t is the turbulent viscosity determined by Baldwin Lomax model. For a laminar flow, the μ_t is set to be zero.

2.2 Time Marching Scheme

The time dependent governing equation (1) is solved using the control volume method with the concept of dual time stepping suggested by Jameson [13]. A pseudo temporal term $\frac{\partial \mathbf{Q}}{\partial \tau}$ is added to the governing equation (1). This term vanishes at the end of each physical time step, and has no influence on the accuracy of the solution. However, instead of using the explicit scheme as in [13], an implicit pseudo time marching scheme using line Gauss-Seidel iteration is employed to achieve high CPU efficiency. For unsteady time accurate computations, the temporal term is discretized implicitly using a three point, backward differencing as the following

$$\frac{\partial \mathbf{Q}}{\partial t} = \frac{3Q^{n+1} - 4Q^n + Q^{n-1}}{2\Delta t} \tag{13}$$

Where n is the time level index. The pseudo temporal term is discretized with first order Euler scheme. Let m stand for the iteration index within a physical time step, the semi-discretized governing equation (1) can be expressed as

4

$$[(\frac{1}{\Delta\tau} + \frac{1.5}{\Delta t})I - (\frac{\partial R}{\partial Q})^{n+1,m}]\delta Q^{n+1,m+1} = R^{n+1,m} - \frac{3Q^{n+1,m} - 4Q^n + Q^{n-1}}{2\Delta t} \tag{14}$$

where the $\Delta\tau$ is the pseudo time step, R is the net flux going through the control volume,

$$R = -\frac{1}{V}\int_s [(F - F_v)\mathbf{i} + (G - G_v)\mathbf{j} + (H - H_v)\mathbf{k}]\cdot d\mathbf{s} \tag{15}$$

where V is the volume of the control volume, $\mathbf{s}$ is the control volume surface area vector. Equation (14) is solved using the unfactored line Gauss-Seidel iteration. Two line sweeps in each pseudo time steps are used, one sweeps forward and the other sweeps backforward. The alternative sweep directions are beneficial to the information propagation to reach high convergence rate. Within each physical time step, the solution marches in pseudo time until converged. The method is unconditionally stable and can reach very large pseudo time step since no factorization error is introduced.

2.3   The Zha E-CUSP2 scheme on a moving grid system

To clearly describe the formulations, the vectors $\mathbf{Q}$ and $\mathbf{E}'$ in Eq. (1) are given below:

$$\mathbf{Q} = \begin{pmatrix} \bar{\rho} \\ \bar{\rho}\tilde{u} \\ \bar{\rho}\tilde{v} \\ \bar{\rho}\tilde{w} \\ \bar{\rho}\tilde{e} \end{pmatrix}, \quad \mathbf{E}' = \frac{1}{J}\hat{\mathbf{E}}, \quad \hat{\mathbf{E}} = \begin{pmatrix} \bar{\rho}\tilde{U} \\ \bar{\rho}\tilde{u}\tilde{U} + \xi_x\tilde{p} \\ \bar{\rho}\tilde{v}\tilde{U} + \xi_y\tilde{p} \\ \bar{\rho}\tilde{w}\tilde{U} + \xi_z\tilde{p} \\ \bar{\rho}\tilde{e}\tilde{U} + \tilde{p}\bar{U} \end{pmatrix} \tag{16}$$

$\tilde{U}$ is the contravariant velocity in ξ direction and is defined as the following:

$$\tilde{U} = \xi_t + \xi_x\tilde{u} + \xi_y\tilde{v} + \xi_z\tilde{w} \tag{17}$$

$\bar{U}$ is defined as:

$$\bar{U} = \tilde{U} - \xi_t \tag{18}$$

The Jacobian matrix $\hat{\mathbf{A}}$ is defined as:

$$\hat{\mathbf{A}} = \frac{\partial\hat{\mathbf{E}}}{\partial\mathbf{Q}} = \hat{\mathbf{T}}\hat{\mathbf{\Lambda}}\hat{\mathbf{T}}^{-1} \tag{19}$$

where $\hat{\mathbf{T}}$ is the right eigenvector matrix of $\hat{\mathbf{A}}$, and $\hat{\mathbf{\Lambda}}$ is the eigenvalue matrix of $\hat{\mathbf{A}}$ on the moving grid system with the eigenvalues of:

$$(\tilde{U} + \tilde{C}, \tilde{U} - \tilde{C}, \tilde{U}, \tilde{U}, \tilde{U}) \tag{20}$$

where $\tilde{C}$ is the speed of sound corresponding to the contravariant velocity:

$$\tilde{C} = c\sqrt{\xi_x^2 + \xi_y^2 + \xi_z^2} \tag{21}$$

and where $c = \sqrt{\gamma RT}$ is the physical speed of sound.

Due to the homogeneous relationship between $\mathbf{Q}$ and $\hat{\mathbf{E}}$, the following formulation applies:

$$\hat{\mathbf{E}} = \hat{\mathbf{A}}\mathbf{Q} = \hat{\mathbf{T}}\hat{\mathbf{\Lambda}}\hat{\mathbf{T}}^{-1}\mathbf{Q} \tag{22}$$

In an E-CUSP scheme, the eigenvalue matrix is split as the following:

$$\hat{\mathbf{\Lambda}} = \begin{pmatrix} \tilde{U} - \tilde{C} & 0 & 0 & 0 & 0 \\ 0 & \tilde{U} & 0 & 0 & 0 \\ 0 & 0 & \tilde{U} & 0 & 0 \\ 0 & 0 & 0 & \tilde{U} & 0 \\ 0 & 0 & 0 & 0 & \tilde{U} + \tilde{C} \end{pmatrix} = \tilde{U}[\mathbf{I}] + \begin{pmatrix} -\tilde{C} & 0 & 0 & 0 & 0 \\ 0 & 0 & 0 & 0 & 0 \\ 0 & 0 & 0 & 0 & 0 \\ 0 & 0 & 0 & 0 & 0 \\ 0 & 0 & 0 & 0 & \tilde{C} \end{pmatrix} \tag{23}$$

The grid velocity term $\xi_t[\mathbf{I}]$ due to the moving mesh is naturally included in the convective term, $\tilde{U}$, as given in Eq. (17). Therefore, Eq. (22) becomes:

$$\hat{\mathbf{E}} = \hat{\mathbf{T}}\{\tilde{U}[\mathbf{I}] + \begin{pmatrix} -\tilde{C} & 0 & 0 & 0 & 0 \\ 0 & 0 & 0 & 0 & 0 \\ 0 & 0 & 0 & 0 & 0 \\ 0 & 0 & 0 & 0 & 0 \\ 0 & 0 & 0 & 0 & \tilde{C} \end{pmatrix}\}\hat{\mathbf{T}}^{-1}\mathbf{Q} = \hat{\mathbf{E}}^c + \hat{\mathbf{E}}^p$$

$$= \begin{pmatrix} \bar{\rho}\tilde{U} \\ \bar{\rho}\tilde{u}\tilde{U} \\ \bar{\rho}\tilde{v}\tilde{U} \\ \bar{\rho}\tilde{w}\tilde{U} \\ \bar{\rho}\tilde{e}\tilde{U} \end{pmatrix} + \begin{pmatrix} 0 \\ \xi_x\tilde{p} \\ \xi_y\tilde{p} \\ \xi_z\tilde{p} \\ \tilde{p}\bar{U} \end{pmatrix} \tag{24}$$

where $\hat{\mathbf{E}}^{\mathbf{c}}$ and $\hat{\mathbf{E}}^{\mathbf{p}}$ are namely the convective and pressure fluxes. As shown above, the way of splitting the total flux into convective and pressure fluxes in an E-CUSP scheme is purely based on the analysis of characteristics of the system. As shown in Eq. (24), the convective flux has the upwind characteristic $\tilde{U}$ and is only associated with the convective velocity. The pressure flux has a downwind and an upwind characteristic and it completely depends on the propagation of an acoustic wave.

The Zha E-CUSP2 scheme is based on the E-CUSP scheme suggested by Zha and Hu [10], which is extended to a moving mesh system by the following:

$$\hat{\mathbf{E}}_{\frac{1}{2}} = \frac{1}{2}[(\bar{\rho}\tilde{U})_{\frac{1}{2}}(\mathbf{q^c}_L + \mathbf{q^c}_R) - |\bar{\rho}\tilde{U}|_{\frac{1}{2}}(\mathbf{q^c}_R - \mathbf{q^c}_L)] +$$

$$
\begin{pmatrix}
0 \\
P^+ p\tilde{\xi}_x \\
P^+ \tilde{p}\xi_y \\
P^+ \tilde{p}\xi_z \\
\frac{1}{2}\tilde{p}(\bar{U} + \bar{C}_{\frac{1}{2}})
\end{pmatrix}_L
+
\begin{pmatrix}
0 \\
P^- \tilde{p}\xi_x \\
P^- \tilde{p}\xi_y \\
P^- \tilde{p}\xi_z \\
\frac{1}{2}\tilde{p}(\bar{U} - \bar{C}_{\frac{1}{2}})
\end{pmatrix}_R
\tag{25}
$$

where

$$
(\bar{\rho}\tilde{U})_{\frac{1}{2}} = (\bar{\rho}_L \tilde{U}_L^+ + \bar{\rho}_R \tilde{U}_R^-)
\tag{26}
$$

$$
\mathbf{q^c} =
\begin{pmatrix}
1 \\
\tilde{u} \\
\tilde{v} \\
\tilde{w} \\
\tilde{e}
\end{pmatrix}
\tag{27}
$$

$$
\tilde{C}_{\frac{1}{2}} = \frac{1}{2}(\tilde{C}_L + \tilde{C}_R)
\tag{28}
$$

$$
\tilde{M}_L = \frac{\tilde{U}_L}{\tilde{C}_{\frac{1}{2}}}, \qquad \tilde{M}_R = \frac{\tilde{U}_R}{\tilde{C}_{\frac{1}{2}}}
\tag{29}
$$

$$
\tilde{U}_L^+ = \tilde{C}_{\frac{1}{2}}\{\frac{\tilde{M}_L + |\tilde{M}_L|}{2} + \alpha_L[\frac{1}{4}(\tilde{M}_L + 1)^2 - \frac{\tilde{M}_L + |\tilde{M}_L|}{2}]\}
\tag{30}
$$

$$
\tilde{U}_R^- = \tilde{C}_{\frac{1}{2}}\{\frac{\tilde{M}_R - |\tilde{M}_R|}{2} + \alpha_R[-\frac{1}{4}(\tilde{M}_R - 1)^2 - \frac{\tilde{M}_R - |\tilde{M}_R|}{2}]\}
\tag{31}
$$

$$
\alpha_L = \frac{2(\tilde{p}/\bar{\rho})_L}{(\tilde{p}/\bar{\rho})_L + (\tilde{p}/\bar{\rho})_R}, \qquad \alpha_R = \frac{2(\tilde{p}/\bar{\rho})_R}{(\tilde{p}/\bar{\rho})_L + (\tilde{p}/\bar{\rho})_R}
\tag{32}
$$

$$
P^{\pm} = \frac{1}{4}(\tilde{M} \pm 1)^2(2 \mp \tilde{M}) \pm \alpha\tilde{M}(\tilde{M}^2 - 1)^2, \qquad \alpha = \frac{3}{16}
\tag{33}
$$

$$
\bar{C} = \tilde{C} - \xi_t
\tag{34}
$$

$$
\bar{C}_{\frac{1}{2}} = \frac{1}{2}(\bar{C}_L + \bar{C}_R)
\tag{35}
$$

Please note that, in the energy equation of the pressure splitting, $\bar{U}$ and $\bar{C}$ are used instead of $\tilde{U}$ and $\tilde{C}$. The term $\bar{C}$ is constructed by taking into account the effect of the grid velocity so that the flux will transit from subsonic to supersonic smoothly. When $\xi_t = 0$, Eq. (25) naturally returns to the one for a stationary grid.

For supersonic flow, when $\tilde{U}_L \geq \tilde{C}$, $\hat{\mathbf{E}}_{\frac{1}{2}} = \hat{\mathbf{E}}_L$; when $\tilde{U}_R \leq -\tilde{C}$, $\hat{\mathbf{E}}_{\frac{1}{2}} = \hat{\mathbf{E}}_R$.

The original Zha-Hu scheme is found to have temperature oscillations near the solid wall region when the grids is skewed. Therefore, the scheme used in the present study is the modified version scheme, Zha CUSP2 scheme[9]. In this scheme, the total enthalpy instead of the static pressure is used to calculate the numerical dissipation coefficients for the energy equation as below:

$$\alpha_L = \frac{2(\tilde{H}/\bar{\rho})_L}{(\tilde{H}/\bar{\rho})_L + (\tilde{H}/\bar{\rho})_R}, \quad \alpha_R = \frac{2(\tilde{H}/\bar{\rho})_R}{(\tilde{H}/\bar{\rho})_L + (\tilde{H}/\bar{\rho})_R} \tag{36}$$

Note that Equation (36) is only used for the energy equation. For the continuity and momentum equations, Equation (32) is still used as the smoothing coefficient.

2.4 Boundary Conditions

The boundary conditions for the computation of wing flutter are as follows:

(1) Inlet boundary conditions: The far field boundary is divided into inlet and outlet boundaries. On inlet boundary, it is assumed that the streamwise velocity u is uniform, transverse velocity $v = 0$, and spanwise velocity $w = 0$. Other primitive variables are specified according to the freestream condition except the pressure which is extrapolated from interior.

(2) Outlet boundary conditions: All the flow quantities are extrapolated from interior except the pressure which is set to be its freestream value.

(3) Solid wall boundary conditions: At moving boundary surface, the no-slip condition is enforced by extrapolating the velocity between the phantom and interior cells,

$$u_0 = 2\dot{x}_b - u_1, \qquad v_0 = 2\dot{y}_b - v_1, \qquad w_0 = 2\dot{z}_b - w_1 \tag{37}$$

where u_0, v_0 and w_0 denote the velocity at phantom cell, u_1, v_1 and w_1 denote the velocity at the $1st$ interior cell close to the boundary, and u_b, v_b and w_b are the velocity on the moving boundary.

If the wall surface is in η direction, the other two conditions to be imposed on the solid wall are the adiabatic wall condition and the inviscid normal momentum equation[2] as follows,

$$\frac{\partial T}{\partial \eta} = 0, \quad \frac{\partial p}{\partial \eta} = -\left(\frac{\rho}{\eta_x^2 + \eta_y^2 + \eta_z^2}\right)(\eta_x \ddot{x}_b + \eta_y \ddot{y}_b + \eta_z \ddot{z}_b) \tag{38}$$

2.5 Moving/Deforming Grid Systems

In the fully-coupled computation, the remeshing is performed in each iteration. Therefore, a CPU time efficient algebraic grid deformation method is employed in the computation instead of the commonly-used grid generation method in which the Poisson equation is solved for grid points. For clarity, the remeshing procedure for 2D cases is sketched in Figure 1. This grid deformation procedure is designed in such a way that the far-field boundary (j=jlp) is held fixed, and the grids on the wing surface (j=1) moves and deforms following the instantaneous motion of the wing structure. After the new wing surface is determined, two components of the displacement vector at wing surface node dx_1 and dy_1 can be calculated accordingly. First, the length of each segment along the old mesh line is estimated as:

$$s_j = s_{j-1} + \sqrt{(x_j - x_{j-1})^2 + (y_j - y_{j-1})^2} \qquad (j = 2, \cdots, jlp) \qquad (39)$$

where $s_1 = 0$ and the displacement vectors at wing surface node (dx_1, dy_1) and at the far-field boundary (dx_{jlp}, dy_jlp) are known. Then the grid node points between the wing surface and the far-field boundary can be obtained by using following linear interpolation:

$$dx_j = \frac{dx_{jlp} - dx_1}{s_{jlp} - s_1} s_j + \frac{dx_1 s_{jlp} - dx_{jlp} s_1}{s_{jlp} - s_1} \qquad (40)$$

$$dy_j = \frac{dy_{jlp} - dy_1}{s_{jlp} - s_1} s_j + \frac{dy_1 s_{jlp} - dy_{jlp} s_1}{s_{jlp} - s_1} \qquad (41)$$

This simple remeshing strategy is proved to be robust for all the cases investigated in present study. By monitoring the accuracy criterion y^+, it is shown that the method can maintain the initial grid quality and keep almost the same mesh distribution around the wing surface.

For 3D case, the Equation (42) becomes

$$s_j = s_{j-1} + \sqrt{(x_j - x_{j-1})^2 + (y_j - y_{j-1})^2 + (z_j - z_{j-1})^2} \qquad (j = 2, \cdots, jlp) \qquad (42)$$

and one more equation is added to determined the z component of displacement vector:

$$dz_j = \frac{dz_{jlp} - dz_1}{s_{jlp} - s_1} s_j + \frac{dz_1 s_{jlp} - dz_{jlp} s_1}{s_{jlp} - s_1} \qquad (43)$$

2.6 Geometric Conservation Law

It was pointed out by Thomas et al.[14] that due to the mixed temporal and spatial derivatives after discretization, an additional term appears, which theoretically equals to zero but numerically still remains. Consequently numerical error could be introduced in the discretized form of the equations of the flow motion if this term is neglected. In order to reduce or avoid this error, the geometric conservation law needs to be enforced. In other words, the following additional term should be added to the right-hand side of the equations as a source term:

$$\mathbf{S} = \mathbf{Q} \left[\frac{\partial J^{-1}}{\partial t} + \left(\frac{\xi_t}{J} \right)_\xi + \left(\frac{\eta_t}{J} \right)_\eta + \left(\frac{\zeta_t}{J} \right)_\zeta \right] \qquad (44)$$

To implement this option in the flow solver, the source term is then linearized such that

$$\mathbf{S}^{n+1} = \mathbf{S}^n + \frac{\partial \mathbf{S}}{\partial \mathbf{Q}} \Delta \mathbf{Q}^{n+1} \qquad (45)$$

As has been observed in ref.[15], the overall performance of this numerical supplement is beneficial with very little CPU time cost.

3 Structural Model of Three Dimensional Wing

The governing equation of the solid structure motion can be written as,

$$\mathbf{M}\frac{d^2\mathbf{u}}{dt^2} + \mathbf{C}\frac{d\mathbf{u}}{dt} + \mathbf{K}\mathbf{u} = \mathbf{f} \tag{46}$$

where $\mathbf{M}$, $\mathbf{C}$ and $\mathbf{K}$ are the mass, damping, and stiffness matrices of the solid respectively, $\mathbf{u}$ is the displacement vector and $\mathbf{f}$ is the force exerted on the surface node points of the solid, both can be expressed as:

$$\mathbf{u} = \begin{pmatrix} \mathbf{u}_1 \\ \vdots \\ \mathbf{u}_i \\ \vdots \\ \mathbf{u}_N \end{pmatrix}, \mathbf{f} = \begin{pmatrix} \mathbf{f}_1 \\ \vdots \\ \mathbf{f}_i \\ \vdots \\ \mathbf{f}_N \end{pmatrix},$$

where N is the total number of node points of the structural model, $\mathbf{u}_i$ and $\mathbf{f}_i$ are vectors with 3 components in x, y, z directions:

$$\mathbf{u}_i = \begin{pmatrix} \mathbf{u}_{ix} \\ \mathbf{u}_{iy} \\ \mathbf{u}_{iz} \end{pmatrix}, \mathbf{f}_i = \begin{pmatrix} \mathbf{f}_{ix} \\ \mathbf{f}_{iy} \\ \mathbf{f}_{iz} \end{pmatrix}.$$

$\mathbf{f}_i$ is dynamic force exerted on the surface of the solid body. In a modal approach, the modal decomposition of the structure motion can be expressed as follows:

$$\mathbf{K}\boldsymbol{\Phi} = \mathbf{M}\boldsymbol{\Phi}\boldsymbol{\Lambda} \tag{47}$$

or

$$\mathbf{K}\phi_j = \lambda_j\mathbf{M}\phi_j \tag{48}$$

where $\boldsymbol{\Lambda}$ is eigenvalue matrix, $\boldsymbol{\Lambda} = diag[\lambda_1, \cdots, \lambda_j, \cdots, \lambda_{3N}]$, and jth eigenvalue $\lambda_j = \omega_j{}^2$, ω_j is the natural frequency of jth mode, and the mode shape matrix $\boldsymbol{\Phi} = [\phi_1, \cdots, \phi_j, \cdots, \phi_{3N}]$.

Equation (48) can be solved by using a finite element solver (e.g. ANSYS) to obtain its finite number of mode shapes ϕ_j. The first five mode shapes will be used in this paper to calculate the displacement of the structure such that,

$$\mathbf{u}(t) = \sum_j a_j(t)\phi_j = \boldsymbol{\Phi}\mathbf{a} \tag{49}$$

where $\mathbf{a} = [a_1, a_2, a_3, a_4, a_5]^T$. Substitute Equation (49) to Equation (46) and yield

$$\mathbf{M}\boldsymbol{\Phi}\frac{d^2\mathbf{a}}{dt^2} + \mathbf{C}\boldsymbol{\Phi}\frac{d\mathbf{a}}{dt} + \mathbf{K}\boldsymbol{\Phi}\mathbf{a} = \mathbf{f} \tag{50}$$

10

Multiply Equation (50) by $\mathbf{\Phi}^T$ and re-write it as

$$\hat{\mathbf{M}}\frac{d^2\mathbf{a}}{dt^2} + \hat{\mathbf{C}}\frac{d\mathbf{a}}{dt} + \hat{\mathbf{K}}\mathbf{a} = \mathbf{P} \tag{51}$$

where $\mathbf{P} = [P_1, P_2, \cdots, P_j, \cdots, P_N]^T$, the modal force of jth mode, $P_j = \phi_j^T\mathbf{f}$, the modal mass matrix is defined as

$$\hat{\mathbf{M}} = \mathbf{\Phi}^T\mathbf{M}\mathbf{\Phi} = diag(m_1, \cdots, m_j, \cdots, m_{3N}) \tag{52}$$

where m_j is the modal mass of jth mode, and the modal damping matrix is defined as

$$\hat{\mathbf{C}} = \mathbf{\Phi}^T\mathbf{C}\mathbf{\Phi} = diag(c_1, \cdots, c_j, \cdots, c_{3N}) \tag{53}$$

where c_j is the modal damping of jth mode, and the modal stiffness matrix is defined as

$$\hat{\mathbf{K}} = \mathbf{\Phi}^T\mathbf{K}\mathbf{\Phi} = diag(k_1, \cdots, k_j, \cdots, k_{3N}) \tag{54}$$

where k_j is the modal stiffness of jth mode. Equation (51) implies

$$\frac{d^2a_j}{dt^2} + 2\zeta_j\omega_j\frac{da_j}{dt} + \omega_j^2 a_j = \frac{\phi_j^T\mathbf{f}}{m_j} \tag{55}$$

where ζ_j is modal damping ratio. Equation (55) is the modal equation of structure motion, and is solved numerically within each iteration. By carefully choosing reference quantities, the normalized equation may be expressed as

$$\frac{d^2a_j}{dt^{*2}} + 2\zeta_j\left(\frac{\omega_j}{\omega_\alpha}\right)\frac{da_j}{dt^*} + \left(\frac{\omega_j}{\omega_\alpha}\right)^2 a_j = \phi_j^{*T}\mathbf{f}^*V^*\left(\frac{b_s}{L}\right)^2\frac{\bar{m}}{v^*} \tag{56}$$

where the dimensionless quantities are denoted by an asterisk, ω_α is the natural frequency in pitch, b_s is the streamwise semichord measured at wing root, L is the reference length, $\bar{m}$ is the measured wing panel mass, v^* is the volume of a conical frustum having streamwise root chord as lower base diameter, streamwise tip chord as upper base diameter, and panel span as height, $V^* = \frac{U_\infty}{b_s\omega_\alpha\sqrt{\bar{\mu}}}$, and U_∞ is the freestream velocity.

Then the equations are transformed to a state form and expressed as:

$$[\mathbf{M}]\frac{\partial\{\mathbf{S}\}}{\partial t} + [\mathbf{K}]\{\mathbf{S}\} = \mathbf{q} \tag{57}$$

where

$$\mathbf{S} = \begin{pmatrix} a_j \\ \dot{a}_j \end{pmatrix}, \mathbf{M} = [I], \mathbf{K} = \begin{pmatrix} 0 & -1 \\ \left(\frac{\omega_j}{\omega_\alpha}\right)^2 & 2\zeta\left(\frac{\omega_j}{\omega_\alpha}\right) \end{pmatrix}, \mathbf{q} = \begin{pmatrix} 0 \\ \phi_j^{*T}\mathbf{f}^*V^*\left(\frac{b_s}{L}\right)^2\frac{\bar{m}}{v^*} \end{pmatrix}.$$

To couple the structural equations with the equations of flow motion and solve them implicitly in each physical time step, above equations are discretized and integrated in a manner consistent with Equation (14) to yield

11

$$\left(\frac{1}{\Delta\tau}\mathbf{I} + \frac{1.5}{\Delta t}\mathbf{M} + \mathbf{K}\right)\delta S^{n+1,m+1} = -\mathbf{M}\frac{3\mathbf{S}^{n+1,m} - 4\mathbf{S}^n + \mathbf{S}^{n-1}}{2\Delta t} - \mathbf{K}\mathbf{S}^{n+1,m} + \mathbf{q}^{n+1,m+1} \qquad (58)$$

where n is the physical time level index while m stands for the pseudo time index. The detailed coupling procedure between the fluid and structural systems is given in the following section.

4   Fully Coupled Fluid-Structural Interaction Procedure

To rigorously simulate fluid-structural interactions, the equations of flow motion and structural response need to be solved simultaneously within each iteration in a fully coupled numerical model. The calculation based on fully coupled iteration is CPU expensive, especially for three dimensional applications. The modal approach can save CPU time significantly by solving modal displacement equations, Equation (55), instead of the original structural equations, Equation (48), which is usually solved by using finite element method. In the modal approach, the structural mode shapes can be pre-determined by using a separate finite element structural solver. Once the several mode shapes of interest are obtained, the physical displacements can be calculated just by solving those simplified linear equations, Equation (55) and Equation (49). In present study, the first five mode shapes provided in Ref.[11] are used to model the wing structure. These pre-calculated mode shapes are obtained on a fixed structural grid system and are transformed to the CFD grid system by using a 3rd order polynomial fitting procedure. The procedure is only performed once and then the mode shapes for CFD grid system are stored in the code throughout the simulation.

The procedure of the fully coupled fluid-structure interaction by modal approach is described as follows:

(1) The flow solver provides dynamic forces on solid surfaces.

(2) Integrate fluid forces at each surface element to obtain the forcing vector $\mathbf{f}$.

(3) Use Equation (55) to calculate modal displacements $a_j(j = 1, 2, 3, 4, 5)$ of the next pseudo time step.

(4) Use Equation (49) to calculate physical displacement $\mathbf{u}$ of the next pseudo time step.

(5) Check the maximum residuals of both solutions of the flow and the structural equations. If the maximum residuals are greater than the prescribed convergence criteria, go back to step (1) and proceed to the next pseudo time. Otherwise the calculation of the flow field and the structural displacement within the physical time step is completed and the next new physical time step starts. The procedure can be also seen in the flow chart given in Figure 2.

5   Results and Discussion

The result of steady state transonic ONERA M6 wing is calculated first in order to validate CFD solver. Then, the flutter boundary of an AGARD wing 445.6 is calculated.

5.1 Steady State Transonic ONERA M6 wing

As a validation of the three dimensional solver for a transonic wing, the steady state solution of the transonic ONERA M6 wing is calculated. The freestream conditions for this study are listed in Table 1 below.

Table 1: Free-stream condition for ONERA M6 wing

Mach number	0.8395
Static Pressure (psia)	12.2913
Temperature (R)	447.0
Angle-of-Attack (deg)	0.0
Reynolds Number	19.7×10^6

This case is calculated using an O-type grid with the dimension of 144 (around wing) $\times 60$ (normal to the wing) $\times 40$ (spanwise). The far field boundary is located 15 chords away from the chord center of the wing. The surface mesh of the wing is depicted in Figure 3.

The Zha E-CUSP2 scheme is used to evaluate the inviscid fluxes with the 3rd order MUSCL type differencing [16]. The turbulent Reynolds stress and heat flux are calculated by the Baldwin-Lomax algebraic model[12].

The computed surface pressure distributions at various cross sections are shown in Figure 4, together with the experimental data given by Schmitt et al. [17]. The location of $z/b = 0.2$ is near the root, and $z/b = 0.99$ is at wing tip.

Overall, very good agreement is obtained between the computation and experiment for each cross-section.

5.2 Other Validations

The code has been intensively validated for the 2D fluid-structure interaction cases [18]. The modal approach solver is validated with a finite element solver in [8]. The results agree excellently.

5.3 AGARD Wing 445.6 Flutter

The AGARD 445.6 wing is selected to demonstrate the capability of the present solver for predicting the flutter boundary. This wing has a quarter-chord sweep angle of 45 degree, an aspect ratio of 1.65, a taper ratio of 0.6576, and a NACA65A004 airfoil section in the streamwise direction. The weakened wing model (Model 3) listed in [11] is chosen for this study. The geometry of the wing and its first six mode shapes as well as the experimental flutter results are also provided in the same report [11]. The wing structure is modeled by its first five natural vibration modes in the present computation.

The simulations start with the stationary rigid body wing model. After the steady state flow field around the wing is fully developed, the rigid body wing is switched to the flexible wing model. As a small imposed perturbation, the first mode displacement of the structural motion is set into sinusoidal motion for one cycle with the maximum amplitude of 0.0005 - 0.001 and the first mode

frequency of the wing. Then the wing is allowed to deflect in response to the dynamic force load. Within each physical time step, the solution is usually converged within 50 iterations.

In Figures 5 through 7 the time histories of generalized displacements of the AGARD wing 445.6 at $M_\infty = 0.96$ are plotted for three different V^*. In these figures, from $V^* = 0.26$ to $V^* = 0.315$, the plots correspond to the damped, neutral, and diverging responses, respectively. When the value of V^* is smaller than the critical value on the flutter boundary, the amplitudes of all modes decrease in time corresponding to the damped response as shown in Figure 5. Once the value of V^* coincides with or is close to the critical value, the neutral response appears as shown in Fig. 6. When the value of V^* is above the neutral stability point, the amplitudes of first five modes grow very fast, a diverging response is reached as shown in Fig. 7.

For a given Mach number, several runs with different V^* are needed to determine the location of the flutter boundary using bisection method. When V^* is varied, the free-stream Reynolds number is changed accordingly. Strictly speaking, the free-stream Reynolds number needs to be updated and the initial steady-state flow field with actual Reynolds number should be re-generated for each run. In present simulation, the initial flow field and the Reynolds number remain unchanged when V^* is varied since the effect on final solution due to small variation in the free-stream Reynolds number is negligible when a turbulence model is used.

The comparison of computed flutter boundary and experimental data for AGARD Wing 445.6 is illustrated in Figure 8. Overall, the computed results are in good agreement with the experimental data. The "sonic dip" near Mach = 1.0 measured in the experiment is very well captured by the computation. The discrepancy between computed results and experimental data may be due to the inadequacy of the turbulent modeling to capture the shock/wave boundary layer interaction or may be due to the inaccurate measurement in the experiment as suspected by some researchers.

6   Conclusion

An aeroelastic solver using the newly-proposed efficient high resolution Zha E-CUSP2 upwind scheme for predicting 3-D wing flutter boundary has been developed. The 3D Reynolds average Navier-Stokes equations are solved. Closure of the Reynolds stresses is provided by the Baldwin-Lomax turbulence model. The modal approach solver is used to calculate the structural response under aerodynamic forces with second-order accuracy. The CFD and structural solvers are fully coupled implicitly via successive iterations within each physical time step. The numerical results show that this method is capable of capturing the aeroelastic properties of the flexible wing efficiently. The computed flutter boundary of AGARD Wing 445.6 for free stream Mach numbers ranging from 0.499 to 1.141 agrees well with the experiment.

7   Acknowledgment

References

[1] E. Lee-Rausch and J. Batina, "Calculation of AGARD Wing 445.6 Flutter Using Navier-Stokes Aerodynamics." AIAA Paper 93-3476, August 9-11, 1993.

[2] S. A. Morton, R. B. Melville, and M. R. Visbal, "Accuracy and Coupling Issues of Aeroelastic Navier-Stokes Solutions on Deforming Meshes." AIAA Paper-97-1085, 1997.

[3] R. B. Melville, S. A. Morton, and D. P. Rizzetta, "Implementation of a Fully-Implicit, Aeroelastic Navier-Stokes Solver." AIAA Paper-97-2039, 1997.

[4] R. B. Melville and S. A. Morton, "Fully Implicit Aeroelasticity on Oveerset Grid Systems ." AIAA Paper-98-0521, 1998.

[5] R. Gordnier and M. R.B., "Transonic Flutter Simulations Using an Implicit Aeroelastic Solver," *Journal of Aircraft*, vol. 37, pp. 872–879, September-October 2000.

[6] F. Liu, J. Cai, Y. Zhu, A. Wong, and H. Tsai, "Calculation of Wing Flutter by a Coupled CFD-CSD Method." AIAA-2000-0907, 2000.

[7] H. Doi and J. Alonso, "Fluid/Structure Coupled Aeroelastic Computations for Transonic Flows in Turbomachinery." ASME Turbo Expo 2002, GT-2002-30313, 2002.

[8] X.-Y. Chen, G.-C. Zha, and M.-T. Yang, "Numerical Simulation of 3-D Wing Flutter with Fully Coupled Fluid-Structure Interaction Approach." AIAA Paper 2006-0697, 2006, submitted to Journal of Computers and Fluids.

[9] G.-C. Zha, "A Low Diffusion Efficient Upwind Scheme," *AIAA Journal*, vol. 43, pp. 1137–1140, May 2005.

[10] G.-C. Zha and Z.-J. Hu, "Calculation of Transonic Internal Flows Using an Efficient High Resolution Upwind Scheme," *AIAA Journal*, Feb. 2004.

[11] E. Yates Jr., "Agard standard aeroelastic configurations for dynamic response i.-wing 445.6," Tech. Rep. AGARD Report No.765, AGARD, September 1985.

[12] B. Baldwin and H. Lomax, "Thin-Layer Approximation and Algebraic Model for Separated Turbulent flows." AIAA Paper 78-257, 1978.

[13] A. Jameson, "Time Dependent Calculations Using Multigrid with Application to Unsteady Flows past Airfoils and Wings." AIAA Paper 91-1596, 1991.

[14] P. Thomas and C. Lombard, "Geometric Conservation Law and Its Application to Flow Computations on Moving Grids," *AIAA Journal*, vol. 17, pp. 1030–1037, 1979.

[15] X.-Y. Chen, G.-C. Zha, and Z.-J. Hu, "Numerical Simulation of Flow Induced Vibration Based on Fully Coupled-Structural Interactions." AIAA Paper 2004-2240, Juun 28 - July 1, 2004.

[16] B. Van Leer, "Towards the Ultimate Conservative Difference Scheme, III," *Journal of Computational Physics*, vol. 23, pp. 263–75, 1977.

[17] V. Schmitt and F. Charpin, "Pressure Distributions on the onera-m6-wing at Transonic Mach Numbers," Tech. Rep. AGARD AR 138, AGARD, May 1979.

[18] X.-Y. Chen and G.-C. Zha, "Fully Coupled Fluid-Structural Interactions Using an Efficient High Resolution Upwind Scheme," *Journal of Fluids and Structures*, vol. 20, pp. 1105–1125, November 2005.
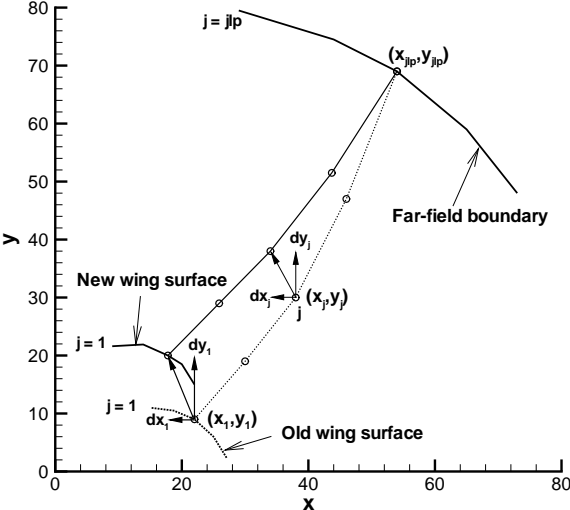
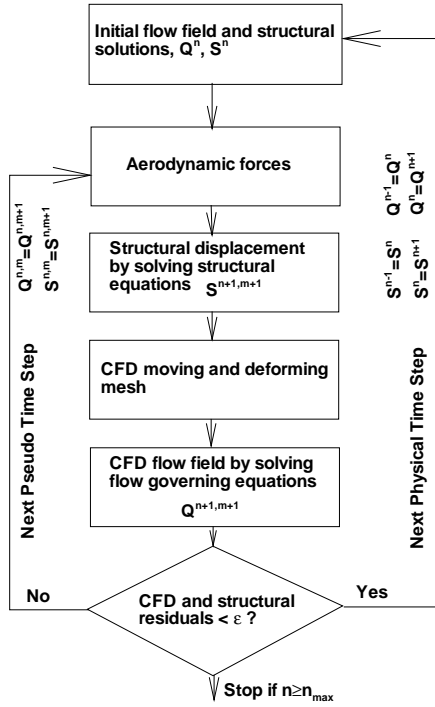Figure 1: A sketch of the mesh deformation

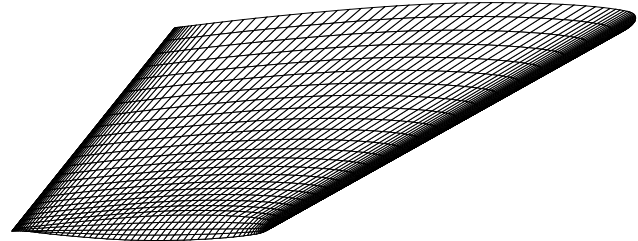Figure 2: Fully coupled flow-structure interaction calculation procedure

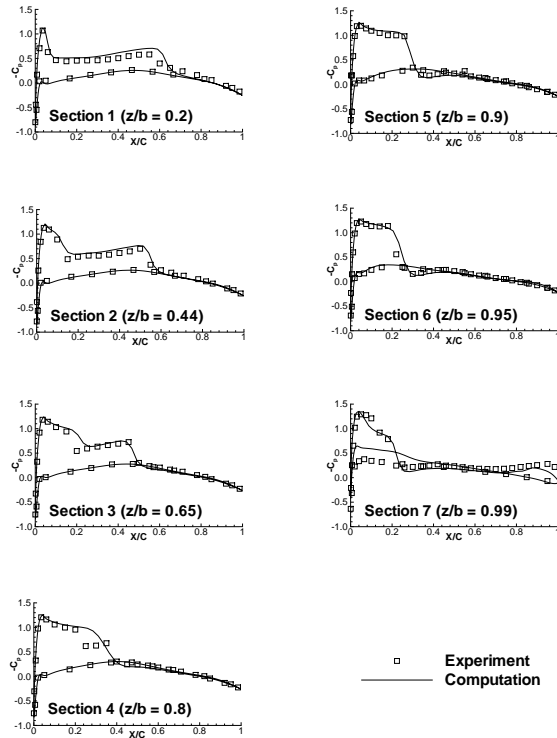Figure 3: The mesh around the ONERA M6 wing surface.

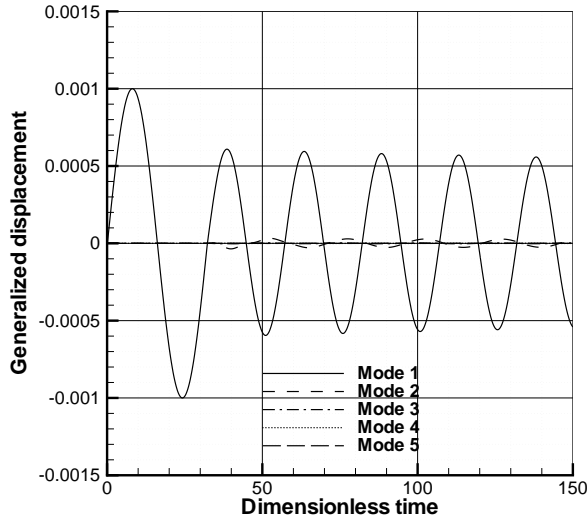Figure 4: Pressure coefficients on the wing surface at different cross-section.

Figure 5: Time histories of the generalized displacements of first five modes for $M_\infty = 0.96$ and $V^* = 0.26$ - Damped response.
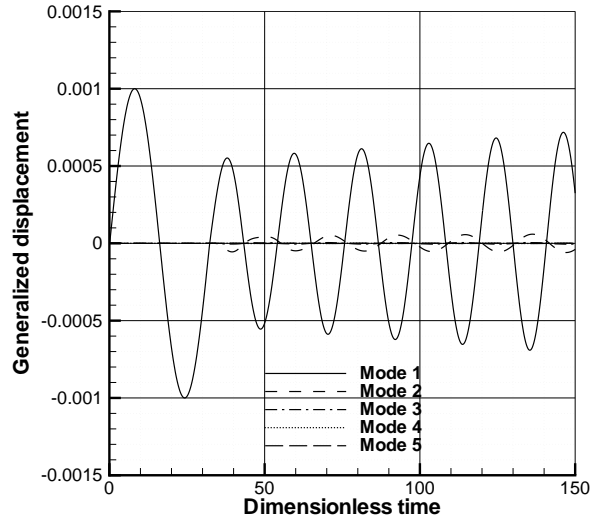

Figure 7: Time histories of the generalized displacements of first five modes for $M_\infty = 0.96$ and $V^* = 0.315$ - Diverging response.
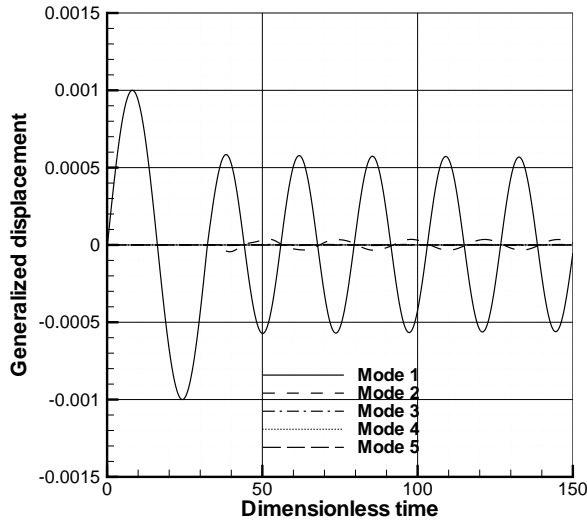

Figure 6: Time histories of the generalized displacements of first five modes for $M_\infty = 0.96$ and $V^* = 0.285$ - Neutrally stable response.
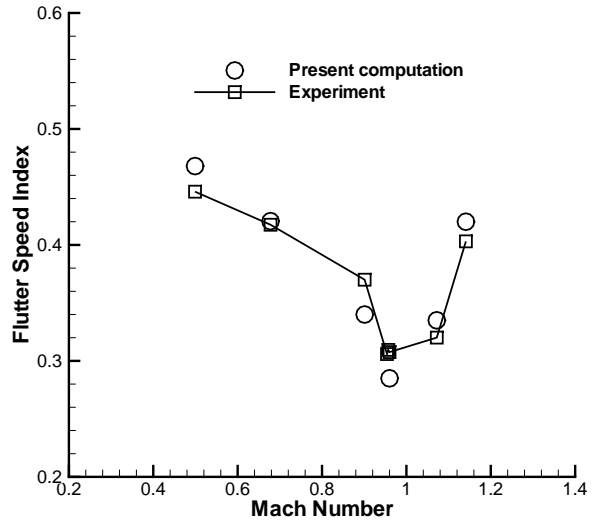

Figure 8: Comparison of predicted wing flutter boundary with experimental data for AGARD Wing 445.6.

18